The Evolution of Climate Sensitivity and Climate Feedbacks in the Community Atmosphere Model

A. GETTELMAN AND J. E. KAY

National Center for Atmospheric Research, Boulder, Colorado*

K. M. SHELL

Oregon State University, Corvallis, Oregon

(Manuscript received 8 April 2011, in final form 26 August 2011)

ABSTRACT

The major evolution of the National Center for Atmospheric Research Community Atmosphere Model (CAM) is used to diagnose climate feedbacks, understand how climate feedbacks change with different physical parameterizations, and identify the processes and regions that determine climate sensitivity. In the evolution of CAM from version 4 to version 5, the water vapor, temperature, surface albedo, and lapse rate feedbacks are remarkably stable across changes to the physical parameterization suite. However, the climate sensitivity increases from 3.2 K in CAM4 to 4.0 K in CAM5. The difference is mostly due to (i) more positive cloud feedbacks and (ii) higher CO_2 radiative forcing in CAM5. The intermodel differences in cloud feedbacks are largest in the tropical trade cumulus regime and in the midlatitude storm tracks. The subtropical stratocumulus regions do not contribute strongly to climate feedbacks owing to their small area coverage. A ''modified Cess'' configuration for atmosphere-only model experiments is shown to reproduce slab ocean model results. Several parameterizations contribute to changes in tropical cloud feedbacks between CAM4 and CAM5, but the new shallow convection scheme causes the largest midlatitude feedback differences and the largest change in climate sensitivity. Simulations with greater cloud forcing in the mean state have lower climate sensitivity. This work provides a methodology for further analysis of climate sensitivity across models and a framework for targeted comparisons with observations that can help constrain climate sensitivity to radiative forcing.

1. Introduction

The earth's climate system is being perturbed by anthropogenic radiative forcing. In addition to direct radiative forcing of the system (e.g., from anthropogenic greenhouse gases), the responses to radiative forcing (surface and atmospheric temperature changes) cause feedbacks within the system that amplify or damp the changes (Schneider 1972; Cess et al. 1990; Bony et al. 2006). Increases in temperature allow the specific humidity to increase, which increases the greenhouse effect due to water vapor (the water vapor feedback). Melting of snow or sea ice lowers the surface albedo, resulting in more absorption of solar radiation (the surface albedo feedback). Increases in surface and atmospheric temperature cause more emission to space, a cooling effect (temperature feedbacks). Clouds exert complex feedbacks due to their opposite shortwave and longwave effects. Clouds reflect shortwave radiation to space, cooling the planet, but absorb longwave radiation and emit at cooler temperatures, causing warming. Low clouds cool and high clouds warm, with the balance of effects being a net cooling (Stephens 2005). Changes to cloud amount, location, and radiative properties (e.g., optical depth) can exert feedbacks on the system.

Any of these feedbacks may significantly alter the magnitude of the response to radiative forcing. The water vapor feedback, for example, is large and positive (Held and Soden 2000). While it is straightforward to calculate the direct radiative forcing, the feedback response to that

* The National Center for Atmospheric Research is sponsored by the National Science Foundation.

Corresponding author address: A. Gettelman, National Center for Atmospheric Research, 1850 Table Mesa Dr., Boulder, CO, 80305.
E-mail: andrew@ucar.edu

DOI: 10.1175/JCLI-D-11-00197.1

forcing is a complex process to measure and understand. Although there are many physical, chemical, biological, and geological feedbacks that operate on a range of time scales, here we focus on the water vapor, lapse rate/temperature, surface albedo, and cloud feedbacks, which are responsible for much of the uncertainty in future climate projections of the next 100 years (Bony et al. 2006; Solomon et al. 2007). Remaining uncertainties stem from ocean heat uptake, anthropogenic emissions, and carbon cycle changes.

Many authors have decomposed and assessed the relative importance of feedbacks using different methods. Cess et al. (1990, 1996) used simplified perturbation experiments with uniform ±2-K sea surface temperature (SST) changes under July conditions (known as ''Cess'' experiments) to diagnose cloud radiative feedbacks. More comprehensive feedback calculations were performed by Colman (2003), who decomposed feedbacks into different components such as water vapor, temperature, albedo, and clouds and found a negative across-model correlation between water vapor and lapse rate feedbacks. Colman (2003) found agreement between the Cess experiments and calculations using the partial radiative perturbation (PRP) technique of Wetherald and Manabe (1988). Senior and Mitchell (1993) and Ringer et al. (2006) found large differences between assessments of feedbacks from either fully coupled or slab ocean models and Cess experiments. Soden and Held (2006) recently performed feedback calculations using a radiative response (or kernel) method. Soden et al. (2008) showed that the kernel method yielded results equivalent to full PRP calculations.

Cess et al. (1990) were among the first to report that cloud feedbacks explain most intermodel differences in climate feedbacks. This is reiterated in a recent review (Stephens 2005). Bony et al. (2004) separated cloud forcing into dynamic and thermodynamic components, showing that the trade cumulus (moderate subsidence) regime was most important for cloud feedback. Bony and Dufresne (2005) found the biggest spread in model projections of cloud feedback in regions of moderate subsidence with trade cumulus clouds. Webb et al. (2006) confirmed that cloud feedbacks were the major source of spread between models, that low-cloud feedbacks were at least half of the signal, and that they were not confined to tropical low cloud (stratocumulus) regions. Medeiros et al. (2008) used aquaplanet experiments and also found that shallow (or trade) cumulus regimes were most important for cloud feedback. Williams and Webb (2009) used a clustering method and noted that regions with low cloud provided the largest variance in model cloud feedback estimates. Thus, there is consensus that cloud feedbacks (and especially shortwave cloud feedback associated with trade cumulus clouds) are critical for understanding climate sensitivity.

This work uses radiative kernels to analyze climate sensitivity and climate feedbacks in two recent versions of the National Center for Atmospheric Research (NCAR) general circulation model (GCM), the Community Atmospheric Model, versions 4 and 5 (CAM4 and CAM5). CAM is the atmospheric component of the Community Earth System Model (CESM). Shell et al. (2008) analyzed feedbacks in an earlier version of CAM using radiative kernels, and Soden et al. (2008) looked at global feedbacks in a suite of models using radiative kernels. We aim to document the climate sensitivity and climate feedbacks in CAM and how they have changed, as well as to understand what regions, regimes and, processes are responsible for these feedbacks. We also provide a framework that can be used generally for future model analyses and comparisons.

Our methods are described in section 2. We describe the model formulations and experiments in section 3 present results in section 4. Sensitivity tests are performed in section 5, a discussion is in section 6, and conclusions are in section 7.

2. Methodology

We apply radiative kernels calculated offline to the climate response in doubled CO_2 experiments with atmospheric GCMs coupled to slab ocean models (SOMs). In CESM, SOM experiments yield results very similar to atmospheric models coupled to a full dynamic ocean (Bitz et al. 2012). For feedbacks attributed to atmospheric physical parameterizations, the same feedbacks found in the SOM runs can be diagnosed with stand-alone atmosphere model SST perturbation experiments. We then use these experiments to better understand the most critical feedback processes and regimes, which turn out to be related to clouds.

When the earth's energy budget is modified, the planet warms or cools to balance the imposed forcing G and return the top-of-atmosphere (TOA) energy imbalance H to zero. At a given time,

$$H = G - \Delta(F - Q) = G + \Delta R. \qquad (1)$$

The sign convention is such that a positive forcing G corresponds to a warming effect. The forcing can be balanced by an increase in outgoing longwave radiation (F; positive values indicate a cooling effect) or a decrease in absorbed solar radiation (Q; positive values indicate a warming effect) due to the climate response. Thus ΔR is the change in net (shortwave minus longwave) TOA (or

top of model in this case) radiation caused by the climate response. In equilibrium, $H = 0$, so $G = -\Delta R = \Delta(F - Q)$. The climate sensitivity γ determines how much the climate, represented by the global average above-surface temperature T_{as}, needs to change for the TOA fluxes to return to equilibrium:

$$G = \frac{\Delta(F - Q)}{\Delta T_{as}} \Delta T_{as} = -\lambda \Delta T_{as}, \tag{2}$$

where λ is the feedback parameter in units of watts per square meter per kelvin and $\gamma = -G/\lambda$ (K) is the climate sensitivity to a forcing G.

Following Zhang et al. (1994), we assume that, to first order, the total feedback parameter λ is the sum of water vapor q, surface temperature T_s, atmospheric temperature T_a, surface albedo α, and cloud C feedback parameters:

$$\lambda = \lambda_{T_s} + \lambda_{T_a} + \lambda_q + \lambda_C + \lambda_\alpha + \mathrm{NT}, \tag{3}$$

where the nonlinear terms NT are less than 10% (Shell et al. 2008) and each parameter corresponds to the change in TOA radiation [$\Delta R = \Delta(Q - F)$] solely due to the change in that feedback variable in response to a 1-K increase in global average surface air temperature (ΔT_{as} = 1 K). The temperature feedback λ_{T_a} can be separated into components owing to a uniform change in atmospheric temperature with height, the "Planck" feedback λ_{T_p}, and a feedback due to changes in temperature lapse rate λ_{LR}. Thus, in Eq. (3), $\lambda_{T_a} = \lambda_{T_p} + \lambda_{LR}$.

The radiative kernel technique (Soden et al. 2008; Shell et al. 2008) factors the feedback parameter for each climate variable X into two parts by approximating the change in $(Q - F)$ in response to ΔX as linear around some base state. The quantity $[\partial(Q - F)/\partial X] = (\partial R/\partial X)$ is the *radiative kernel*, the change in TOA fluxes due to a standard change in a physical climate variable (the adjoint radiative response). It is calculated using an offline radiative transfer model and depends on the radiative transfer code, as well as the base state, where the base state—and the kernel—are a function of space and time. The *climate response* of the variable is (dX/dT_{as}). The climate response is calculated discretely as $(\Delta X/\Delta T_{as})$, where ΔX is the difference in the climate variable X between the experimental and control GCM simulations. Then the climate feedback parameter λ_X is

$$\lambda_X(x, y, [z], t) = \frac{\partial R}{\partial X} \frac{\Delta X}{\Delta T_{as}}; \tag{4}$$

λ_X is computed for every horizontal grid point (x, y) and altitude (z) for all X except T_s and α, for every month of the year (t). Where the feedback is not single level, the contributions in the vertical (z) can be summed to get the net ΔH for each column. For the water vapor feedback, we use $\ln q$ as the feedback variable because it scales well with the radiation. Lapse rate feedback parameters are determined from the atmospheric temperature kernel and the departure of the atmospheric temperature change from the above-surface temperature change (ΔT_{as}).

Because cloud feedbacks are affected by the state of the climate system, to diagnose cloud feedback we use the change in cloud radiative forcing (CRF) (Ramanathan et al. 1989), adjusted to remove the effects of changing noncloud fields. CRF is the difference between the all-sky TOA flux (all) and the clear-sky TOA flux (clr)—the TOA flux the atmospheric column would have if clouds were removed but all other variables remained the same. For the longwave (LW) $\mathrm{CRF_{LW}} = F_{all} - F_{clr}$, and for the shortwave (SW) $\mathrm{CRF_{SW}} = Q_{all} - Q_{clr}$ so that CRF = $\mathrm{CRF_{LW}} + \mathrm{CRF_{SW}}$. The cloud feedback (CF) can be estimated by taking $\Delta\mathrm{CRF}/\Delta T_{as}$.

However, ΔCRF can be influenced by changes in noncloud variables (Zhang et al. 1994; Colman 2003; Soden et al. 2004). For example, if the surface albedo changes, CRF will change, even if clouds remain the same, because R_{clr} changes. We can thus subtract contributions to ΔCRF due to water vapor, temperature, surface albedo, and forcing (CO_2) changes to obtain the adjusted ΔCRF. The adjusted cloud feedback (ACF) is the adjusted ΔCRF divided by the global average near-surface temperature change (ΔT_{as}). Cloud feedbacks can also be decomposed into SW and LW components (ASCF and ALCF, respectively).

The radiative kernels used in this study were calculated offline with CAM, version 3 (CAM3) (Shell et al. 2008). Soden et al. (2008) have shown globally that the radiative kernels calculated with different models produce similar results, so the use of CAM3 kernels is appropriate.

Finally, we will calculate the climate sensitivity γ for the different runs. First, we calculate an effective feedback parameter λ_{eff} using the total change in forcing and TOA energy imbalance between two runs with different surface temperatures and CO_2 concentrations:

$$\lambda_{eff} = -(G_{CO_2} - H)/\Delta T_{as}, \tag{5}$$

where G_{CO_2} is the radiative forcing. For doubling CO_2 from 280 to 560 ppm by volume (ppmv), $G_{CO_2} = 3.5$ or 3.8 W m^{-2}, depending on the model version (see section 6), and H is the change in TOA imbalance. The effective climate sensitivity (γ_{eff}) is then $\gamma_{eff} = -G_{CO_2}/\lambda_{eff}$. For an equilibrium state ($H = 0$), this reduces to ΔT_{as}. The method allows an estimate of γ from runs that are out of balance ($H \neq 0$). Below we show that, for the same model code in equilibrium (a slab ocean model) and out

TABLE 1. Description of runs used in this study. Run types are either slab ocean model (SOM) or modified Cess (Cess) with horizontal resolution (Res) of either 0.9° × 1.25° (1°) or 1.9° × 2.5°(2°) as described in the text.

Name	Type	Res	Description
CAM4-SOM	SOM	1°	CAM4 physics
CAM4-SOM2	SOM	2°	CAM4 physics
CAM5-SOM	SOM	1°	CAM5.1 physics
CAM5-SOM2	SOM	2°	CAM5.0 physics
CAM4-Cess	Cess	2°	CAM4 physics, equal to CAM4-SOM2
+micro	Cess	2°	CAM4 physics + new microphysics
+macro	Cess	2°	Above + new macrophysics
+rad	Cess	2°	Above + new radiation and cloud optics
+aero	Cess	2°	Above + new aerosol scheme
+PBL	Cess	2°	Above + new PBL
CAM5-Cess	Cess	2°	Above + new shallow Cu scheme = CAM5-SOM2

of balance (specified SST formulation), $\gamma_{\text{eff}} \approx \gamma$. This method is conceptually similar to the regression slope method of Gregory et al. (2004).

Feedbacks with vertical structure are integrated over the troposphere. Here the troposphere is defined as the region with pressures higher than 100 hPa. We use this convention throughout the paper except for lapse rate feedbacks where we use pressures higher than 300 hPa poleward of 30° latitude and pressure higher than 100 hPa equatorward of 30° since lapse rates change in the stratosphere.

In zonal mean figures, we show an ''area weighted'' feedback parameter (using Gaussian weights) in units of petawatts (1 PW = 1×10^{15} W) per degree latitude per kelvin (PW $^{\circ -1}$ K^{-1}). This is simply watts per square meter multiplied by the area of a 1° latitude circle (m^2) at each latitude.

3. Model and run description

a. Model

In this study we focus on changes in the CAM between version 4 (CAM4) and version 5 (CAM5) in CESM. CAM4 is essentially the same as NCAR CAM3 (Collins et al. 2004, 2006) with modifications to the deep convective closure and momentum transport described by Neale et al. (2008). The model features a complete radiative transfer scheme, deep and shallow convection, and bulk stratiform cloud scheme with specified cloud particle sizes and a prescribed distribution of aerosol mass.

CAM5 includes a substantially revised physical parameterization suite over CAM4 (Gettelman et al. 2010; Neale et al. 2010). The only major moist physics parameterization remaining constant between CAM4 and CAM5 is the deep convective parameterization (Neale et al. 2008). CAM5 contains an updated moist boundary layer (Bretherton and Park 2009) and shallow cumulus convection scheme (Park and Bretherton 2009) that improves the simulation of low clouds (Neale et al. 2010). The new two-moment stratiform cloud microphysics scheme (Gettelman et al. 2010; Morrison and Gettelman 2008) includes aerosol activation of cloud drops/crystals for liquid and ice, explicitly treating aerosol–cloud interactions. The new radiation code, the Rapid Radiative Transfer Model for GCMs (Iacono et al. 2008), is a correlated-*K* code that compares better to line-by-line calculations than CAM4 (Iacono et al. 2008). The liquid cloud macrophysical closure is described by Neale et al. (2010) and is more consistent with the convection and microphysics schemes. The aerosol treatment in the model uses a modal-based prognostic scheme similar to that described by Easter et al. (2004), but with only three modes (Aitken, accumulation, and coarse), and is described by Liu et al. (2011), whereas CAM4 uses a prescribed mass-based scheme with direct radiative effects and no interaction with clouds.

b. Run configuration

This work uses two different model configurations. First, we run experiments with CAM coupled to a SOM, and then we perform a series of atmosphere-only perturbation experiments. Each experiment is a pair of runs with identical code but with the concentration of CO_2 set to 280 ppmv in one run and 560 ppmv in the other. These simulations are described below and listed in Table 1.

1) SLAB OCEAN MODEL

We use a series of slab ocean model experiments to elucidate differences between CAM4 (CAM4-SOM) and CAM5 (CAM5-SOM) in a coupled framework. SOM runs have only a single layer thermodynamic ocean and sea ice with specified heat fluxes through the bottom. The SOM configurations are described more fully by Bitz et al. (2012) and differ from the configuration used by Kiehl et al. (2006) to assess climate sensitivity in CAM3 and CCSM3. SOM runs are at least 60 years long and in all cases the atmosphere equilibrates with a perturbation in about 20–30 yr, so we analyze the last 20 years. The results are not sensitive to whether the last 10, 15, or 20 yr are used for analysis.

TABLE 2. Feedbacks (λ_X; W m^{-2} K^{-1}), ALCF and ASCF cloud feedback and γ_{eff} (K) from CAM4 and CAM5 SOM runs and Cess experiments as described in the text.

Simulation	λ_α	λ_{Ts}	λ_{Tp}	λ_{LR}	λ_q	ALCF	ASCF	γ_{eff}
CAM4-SOM (1°)	0.34	−0.66	−2.25	−0.22	1.44	0.22	0.21	3.2
CAM4-SOM2 (2°)	0.36	−0.65	−2.25	−0.18	1.39	0.16	0.27	3.1
CAM4-Cess	0.33	−0.64	−2.21	−0.15	1.31	0.19	0.05	2.8
+micro	0.31	−0.64	−2.21	−0.16	1.34	0.32	−0.08	2.7
+macro	0.31	−0.64	−2.21	−0.17	1.34	0.17	0.07	2.9
+rad	0.32	−0.64	−2.22	−0.18	1.34	0.15	0.20	3.7
+aero	0.31	−0.64	−2.22	−0.19	1.34	0.13	0.24	3.5
+PBL	0.31	−0.64	−2.21	−0.15	1.31	0.16	0.10	2.9
+ShCu = CAM5-Cess	0.29	−0.64	−2.29	−0.15	1.32	−0.05	0.46	4.4
CAM5-SOM2 (2°)	0.30	−0.66	−2.28	−0.27	1.47	0.05	0.47	4.2
CAM5-SOM (1°)	0.31	−0.66	−2.31	−0.30	1.54	0.01	0.50	4.0

The SOM runs are listed in Table 1. They represent a baseline CAM4-SOM run at 0.9° × 1.25° horizontal resolution (hereafter 1°). The CAM4-SOM run represents the released version of CAM4 in the Community Climate System Model version 4 (CCSM4), discussed by Bitz et al. (2012). CAM5-SOM uses the CAM5.1 release code and is run at the same resolution. We also have performed SOM runs at 1.9° × 2.5° resolution (hereafter 2°) for CAM4 (CAM4-SOM2) and CAM5 (CAM5-SOM2), and results were found to be quite similar to the 1° experiments. CAM5-SOM2 includes CAM5.0 code used for the modified Cess experiments.

2) STAND-ALONE EXPERIMENTS

Because we are interested in ''fast'' feedbacks that quickly respond to surface properties (and then cause a slow evolution of those properties), we explore a simplified methodology for investigating perturbations to the earth system. Following Cess et al. (1990), we use a stand-alone atmospheric model and fix the SST to a monthly climatology based on observations (Hurrell et al. 2008). We then perturb the system with a specified ΔSST. Cess et al. (1990, 1996) and others have used a horizontally uniform ±2-K perturbation and constant July conditions. This may not reproduce cloud feedbacks from a SOM or fully coupled model (Senior and Mitchell 1993; Ringer et al. 2006). Instead, we contrast a control and a perturbation experiment as follows. The control uses climatological SST and preindustrial CO_2 concentrations. We calculate the spatial SST perturbation (ΔSST) as the difference between a CAM5-SOM run under doubled CO_2 radiative forcing and a corresponding CAM5-SOM run with preindustrial CO_2. ΔSST is added to the SST climatology each month for the perturbation run while also doubling the CO_2 concentration. Both control and perturbation runs use a full and repeating annual SST cycle. We term this a ''modified Cess'' formulation. Differences between the control and perturbation simulations are used to determine feedbacks. The modified Cess runs reproduce the feedbacks in corresponding SOM runs (see Table 2 and the next section).

These runs allow us to rapidly test the effects of changes to the atmospheric physical parameterization suite, as they come to equilibrium in just a few years. While 2 × 60 years are desirable for SOM runs, modified Cess runs can be performed with 2 × 6 years of simulation. Table 1 describes a series of modified Cess experiments that sequentially add parameterizations to CAM4 until the final atmospheric model code is identical to CAM5. The sequence is determined by model structure and dependencies and broadly represents the development path from CAM4 to CAM5. As noted in Table 1, we sequentially replace the cloud microphysics (micro), the cloud fraction or macrophysics (macro), the radiation code and cloud optics (rad), the aerosol scheme (aero), the planetary boundary layer scheme (PBL), and finally the shallow convection scheme (making the complete CAM5 suite). All modified Cess experiments are run at 2° (1.9° × 2.5°) horizontal resolution and are at least 5 years in length, with the CAM4-Cess and CAM5-Cess experiments both 10 years long.

4. Results

We start by looking at the differences between CAM4 and CAM5 in SOM runs for water vapor feedbacks, exploring temperature (including lapse rate) and surface albedo feedbacks, and finally focusing on cloud feedbacks. In discussing cloud feedbacks, we will examine the effects of individual parameterizations for which CAM4 and CAM5 differ. The sign convention used is that positive denotes a warming and negative denotes a cooling.

Despite the presence of many known amplifying feedbacks, high-latitude feedbacks beyond the albedo

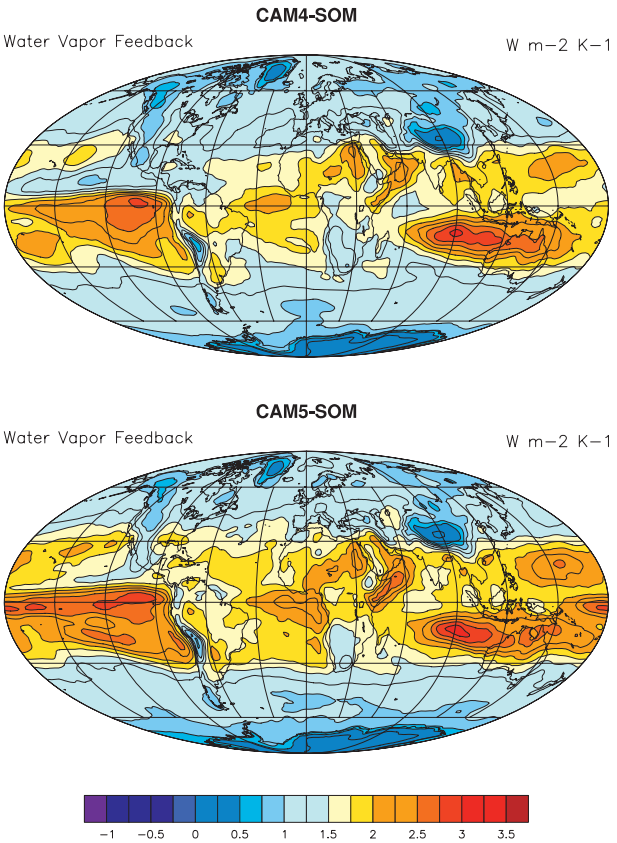

FIG. 1. Vertically integrated tropospheric water vapor feedback (shortwave + longwave) from (top) CAM4 and (bottom) CAM5 SOM experiments.

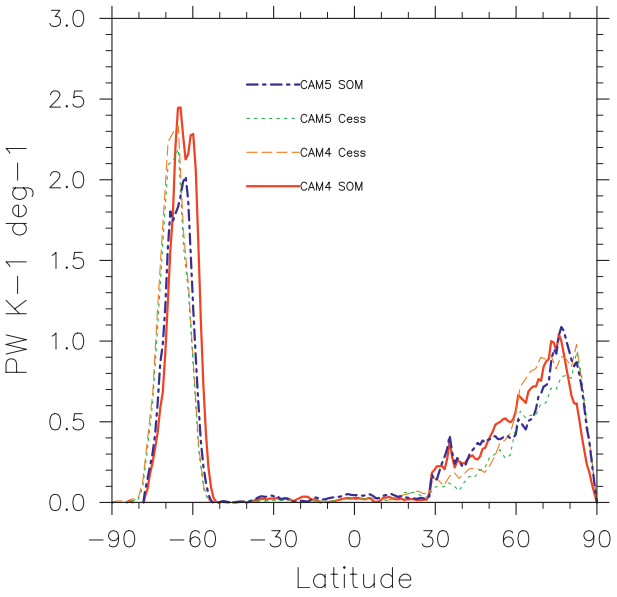

FIG. 2. Zonal-mean shortwave surface albedo feedback (PW K^{-1} $^{o-1}$) from CAM4-SOM (red solid), CAM5-Cess (green dots), CAM4-Cess (orange dash), and CAM5-SOM (blue dot–dash).

feedback are not discussed in great detail here because the high latitudes cover a small fraction of the globe (3% for 70°−90°N or S, 7% for 60°–90°N or S) and therefore are small players in globally averaged feedbacks and feedback differences.

a. Water vapor feedbacks

Figure 1 illustrates the vertically integrated tropospheric water vapor feedback, the sum of SW and LW components, between preindustrial and doubled CO_2 simulations. The globally integrated water vapor feedbacks (Table 2) are nearly the same between CAM4-SOM and CAM5-SOM (1.44 and 1.54 W m^{-2} K^{-1}). For a comparison with other models, see Soden and Held (2006, their Fig. 1). The spatial patterns between CAM5 and CAM4 are similar, with some differences in the tropical Pacific and tropical Atlantic where CAM5 has more positive feedbacks. This is not surprising since the water vapor distributions (and changes) are different in the two simulations. However, the global effect on feedbacks is remarkably stable.

b. Surface temperature, Planck, and lapse rate feedbacks

The atmospheric temperature feedback is divided typically into a component from a uniform temperature change (Planck) and the lapse rate change ($\lambda_{T_a} = \lambda_{T_p} + \lambda_{\mathrm{LR}}$). These feedbacks are similar between the two simulations. The global mean Planck feedback λ_{T_p} is −2.25 for CAM4-SOM and −2.31 W m^{-2} K^{-1} for CAM5-SOM, a difference of 3%. Both models have a surface temperature feedback (λ_{T_s}) of −0.66 W m^{-2} K^{-1}. The lapse rate feedback (λ_{LR}) is −0.22 for CAM4-SOM or −0.30 for CAM5-SOM W m^{-2} K^{-1}. These negative feedbacks act to cool the planet. An increase in temperature leads to increased thermal emission and, hence, damps warming. Spatial patterns of λ_{T_p} and λ_{LR} (not shown) are similar between CAM4 and CAM5. The vertical structure in the two models is also similar for both feedbacks. Lapse rate feedbacks peak in impact in the tropics at 250 hPa because the change in temperature increases with height up to about 250 hPa (Santer et al. 2005). Temperature feedbacks peak at the level where cloud tops are exposed to space (Soden et al. 2008).

The lapse rate feedback difference between the two versions of CAM (−0.08 W m^{-2} K^{-1}) nearly cancels the difference in the water vapor feedback (0.10), in agreement with the result that intermodel differences in the two feedbacks tend to cancel (Colman 2003; Soden and Held 2006).

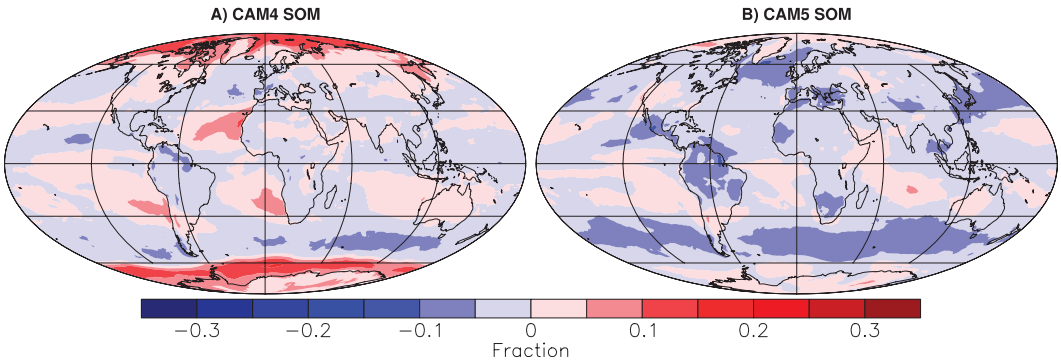

FIG. 3. Change in total cloud fraction ($2 \times CO_2 - 1 \times CO_2$) for (a) CAM4-SOM and (b) CAM5-SOM.

c. *Surface albedo feedbacks*

Surface albedo feedbacks (λ_α) are similar between CAM4 and CAM5 with a difference of 0.03 W m^{-2} K^{-1}, or 9% (Table 2). The zonal mean surface albedo feedbacks for the CAM4 and CAM5 SOM runs are illustrated in Fig. 2 (in PW deg^{-1} K^{-1}). The feedbacks are sharply peaked in the Southern Hemisphere, corresponding to the region of sea ice loss. In the Northern Hemisphere, the region is much broader as both sea ice and land ice and snow contribute. CAM4 has more positive feedbacks in the Southern Hemisphere. In both hemispheres, the regions making large contributions to the albedo feedback in CAM5 tend to be shifted slightly to higher latitudes due to differences in the mean sea ice edge.

d. *Cloud changes*

Table 2 illustrates that the biggest differences between CAM4 and CAM5 are in cloud feedbacks. As an introduction we start by showing the cloud cover changes between $2 \times CO_2$ and $1 \times CO_2$ experiments. Figure 3 shows the change in cloud fraction for CAM4-SOM and CAM5-SOM. Figures 3 and 4 are not normalized for surface temperature changes. Outside of polar regions, CAM5-SOM has much larger changes in cloud fraction than CAM4-SOM. Cloud fraction generally decreases in the warmer ($2 \times CO_2$) CAM5 simulation. The decrease is reflected in the cloud radiative forcing (CRF) changes (Fig. 4). In most locations the forcing change is anticorrelated with fraction change: decreases in cloud fraction reduce the shortwave cooling effects of clouds more than longwave warming and the negative CRF is reduced (a warming effect). There are differences in this correlation over land regions because surface albedo changes play a role in cloud radiative forcing. The change in cloud fraction is often used as a metric for cloud feedbacks (e.g., Stephens (2005)), but this metric can be misleading because cloud optical depth and cloud-top temperature are also important for determining cloud forcing and feedbacks. Cloud fraction and cloud radiative forcing are thus useful but imperfect metrics for understanding cloud feedbacks.

e. *Cloud feedbacks*

Figure 5 shows zonally averaged and area-weighted adjusted cloud feedbacks (ACFs) from CAM4 (thick red line) and CAM5 (dot–dash blue line) SOM runs, as well as from corresponding Cess experiments [CAM5 Cess

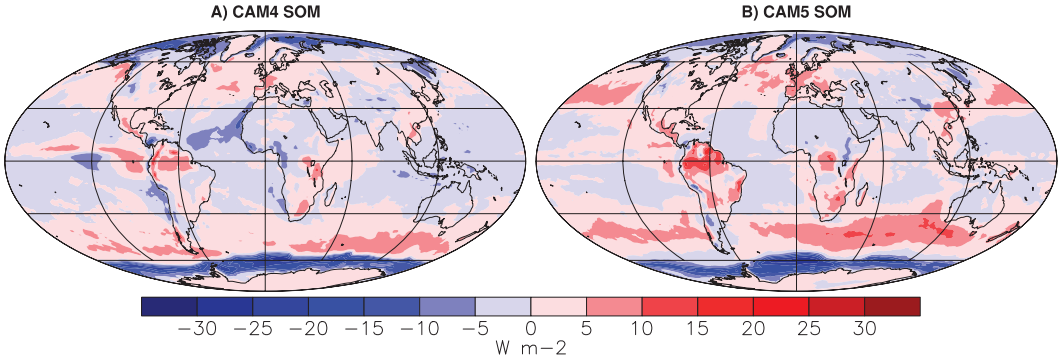

FIG. 4. Change in total longwave plus shortwave (LW + SW) cloud radiative forcing (CRF) ($2 \times CO_2 - 1 \times CO_2$) (W m^{-2}) for (a) CAM4-SOM and (b) CAM5-SOM.

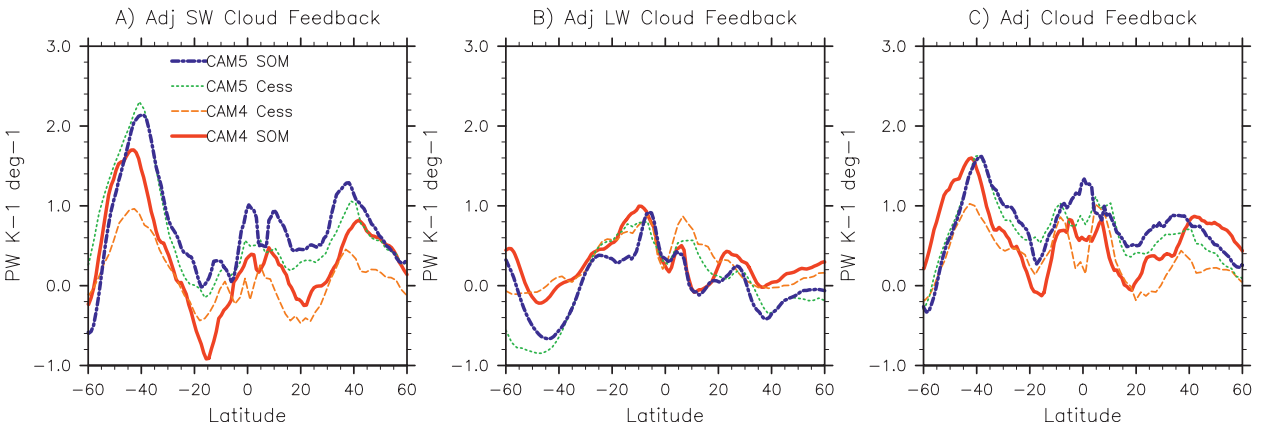

FIG. 5. Zonal-mean adjusted cloud feedback (a) shortwave (ASCF), (b) longwave (ALCF), and (c) total (ACF = ASCF + ALCF) (PW K^{-1} $^{\circ -1}$). Four model runs are shown: SOM runs (thick lines) for CAM4 (red solid) and CAM5 (blue dot–dash), and modified Cess–type experiments (thin lines) for CAM4 (orange dash) and CAM5 (green dots).

(green), CAM4 Cess (orange)]. For clarity, we omit high latitudes poleward of 60° since the area falls off rapidly and the adjustment depends strongly on surface properties (sea ice and snow). These regions have specified sea ice in Cess runs and so are not fully treated by this method.

The adjusted cloud feedbacks (Fig. 5c) between CAM4 and CAM5 differ substantially. The global difference of 0.08 W m^{-2} K^{-1} is nearly 25% of the net feedback (Table 2). Regional differences are large in the subtropics and storm track regions in both hemispheres. In the shortwave (Fig. 5a), there is a large difference between the CAM4 and CAM5 SOM runs at almost all latitudes between 50°S and 40°N. The CAM5-SOM SW cloud feedback is more positive (a warming effect) than CAM4-SOM at almost all latitudes. The largest differences are from 55° to 35°S and from 10° to 40°N. Longwave cloud feedbacks are more negative in CAM5 (a cooling effect), partially compensating the more positive SW feedbacks (Fig. 5b). The SW (Fig. 5a) and net (Fig. 5c) cloud feedbacks in subtropical regions become more positive (20°–30° latitude). The feedbacks imply a net reduction in cloud cooling with increasing temperature in CAM5, also seen in Fig. 4.

Figure 6 shows maps of the adjusted net cloud feedbacks from CAM4 and CAM5 SOM runs (Figs. 6e and 6f). The net positive cloud feedbacks in the Northern Hemisphere midlatitudes, oceans, and the Southern Ocean have increased in strength, while negative feedbacks in the tropics and subtropics have been reduced in CAM5. An examination of cloud fraction (Fig. 3) and cloud forcing (Fig. 4) changes ($2 \times CO_2 - 1 \times CO_2$) indicates that the midlatitude storm track regions have decreasing cloud on their equatorward flanks and increasing cloud at high latitudes in the $2 \times CO_2$ state. As noted in the discussion of the zonal mean changes, there is compensation for deep and high clouds. The reduction of negative cloud forcing in the shortwave (Figs. 6a and 6b) warms, but, in the longwave (Figs. 6c and 6d), the reduction of positive cloud forcing cools.

In the subtropics (10°–30°N and S) there are generally negative SW cloud feedbacks (Figs. 6a and b) in both CAM4 and CAM5. These feedbacks result from regions of increasing low and middle level cloud cover (Fig. 3) and are broadly in trade cumulus regions and near stratocumulus regions on the eastern edges of ocean basins (especially off the western coasts of South America and Africa and in the subtropical Indian Ocean). In CAM5 the negative SW feedback regions (Figs. 6a and 6b), are reduced relative to CAM4. Longwave feedbacks in these regions (Figs. 6c and 6d) are comparable in both models due to increasing midlevel cloud cover in both models (Fig. 3).

In the tropics, CAM5 has reduced negative SW cloud feedbacks over the stratocumulus regions (Figs. 6a and 6b). Strong negative SW cloud forcing changes in stratocumulus regions have been present since at least CAM2 (Stephens 2005). Shortwave feedbacks over deep convective regions vary but are generally positive over tropical land owing to slightly decreasing cloud cover and forcing. The SW cloud feedbacks (Fig. 6a and 6b) dominate the net cloud feedback (Figs. 6e and 6f) over much of the planet. For high clouds, LW feedbacks (Figs. 6c and 6d) can contribute significantly. This occurs in tropical deep convective regions over land, especially over tropical South America and Africa (Figs. 6e and 6f), and tropical oceans (Indian and East Pacific). LW cloud feedbacks can also be important at high latitudes.

Differences in ACF can be broken down by regions and regimes to get a sense of the most important regions

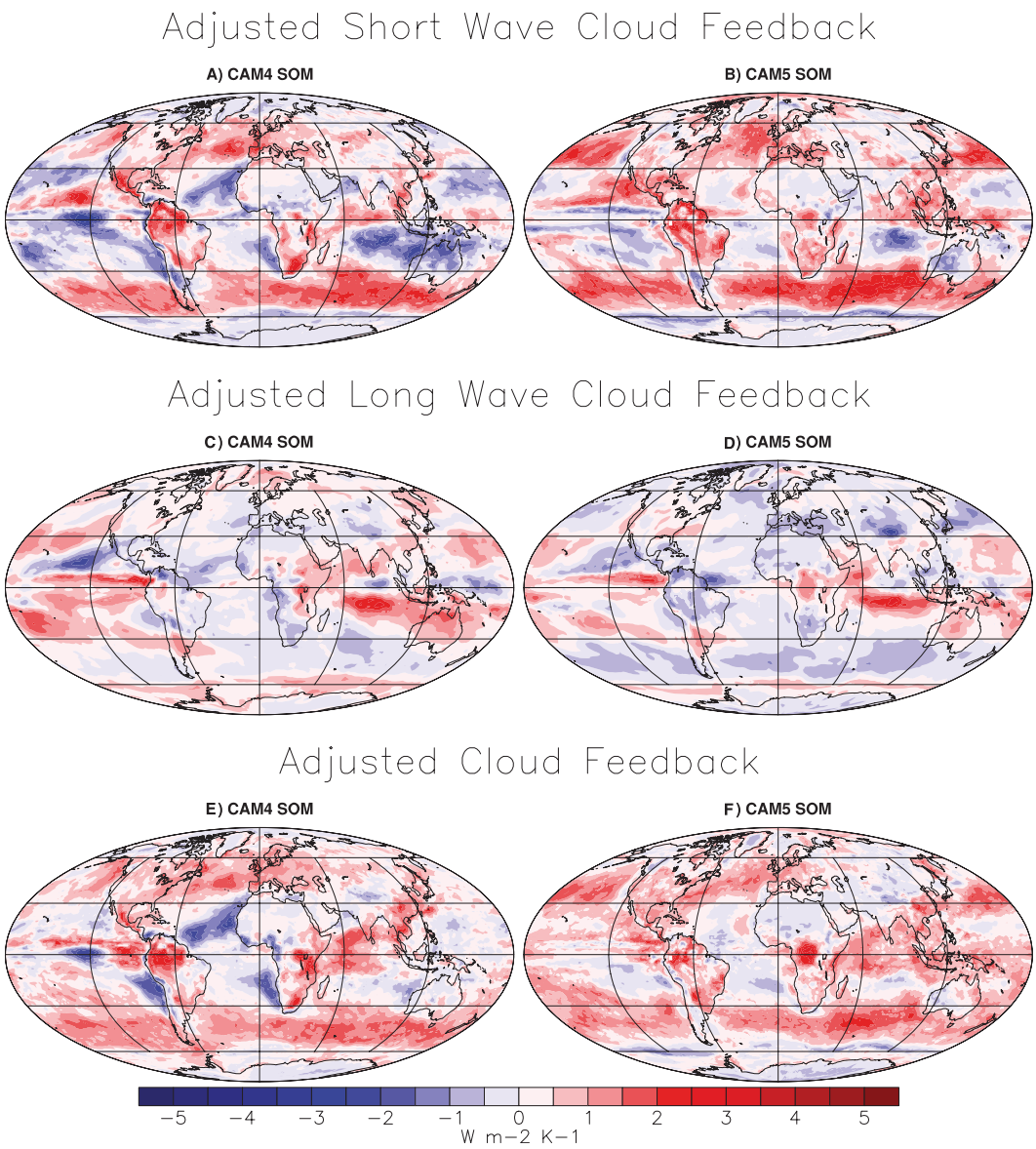

FIG. 6. Adjusted cloud feedback (W m^{-2} K^{-1}) for ASCF in (a) CAM4-SOM and (b) CAM5-SOM, for ALCF in (c) CAM4-SOM and (d) CAM5-SOM, and For net ACF in (e) CAM4-SOM and (f) CAM5-SOM.

for cloud feedbacks and the changes in cloud feedbacks. Figure 7 shows shortwave (Fig. 7a), longwave (Fig. 7b) and net (Fig. 7c) adjusted cloud feedbacks area-weighted so that the total sums to the "global" average value (W m^{-2} K^{-1}). Regions are defined by latitude bands outside of the tropics (90°–60°S, 60°–30°S, 30°–60°N, 60°–90°N). The tropics (|lat| < 30) are divided into regions by 500-hPa vertical velocity (ω_{500mb}) and lower-tropospheric stability (LTS = $\theta_{700mb} - \theta_{surf}$). Tropical regions are defined as (i) deep convection and land (land or $\omega_{500mb} < 0$), (ii) trade cumulus (ocean, $\omega_{500mb} > 0$ and LTS < 17 K) and (iii) stratocumulus (ocean, $\omega_{500mb} > 0$ and LTS > 17 K), following Medeiros and Stevens (2011) and an examination of LTS maps from the simulations. In this context the tropical area is 50% of the planet of which 30% is deep and land, 18% is trade cumulus, and 2% is stratocumulus. The stratocumulus area in CAM4 and CAM5 (2%) is smaller than reanalyses (6%), consistent with model biases that result in breakup of stratocumulus too quickly (Medeiros and Stevens 2011). However, we altered the stability threshold for sorting (to LTS < 15 K) to increase the stratocumulus regions to ~6% of the global area and found that the results are the same.

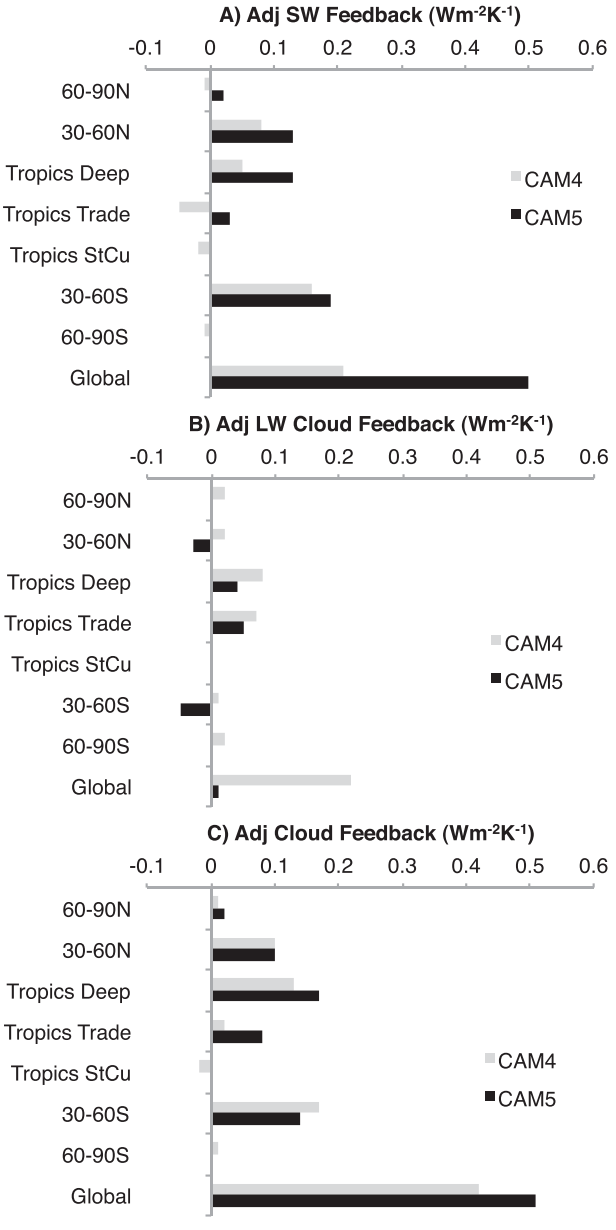

FIG. 7. Weighted ACF (W m^{-2} K^{-1}) by region for CAM4-SOM (gray) and CAM5-SOM (black): (a) ASCF, (b) ALCF, and (c) net (ACF). Regions are defined in the text.

Figure 7c illustrates that adjusted net cloud feedbacks for both CAM4 and CAM5 are dominated by the midlatitude storm tracks (30°–60°N and S) and tropical deep convective (and land) regions. In deep convective regions, cloud fraction decreases slightly (Fig. 3), but the liquid water path increases and cloud tops increase in height. Thus, SW and LW cloud feedbacks are positive. The largest differences between CAM4 and CAM5 are in the tropical deep and trade cumulus regimes (the subtropics), including the equatorward flanks of the storm tracks. CAM5 has positive ASCF in the trade cumulus regime, while CAM4 has negative ASCF (Fig. 7a). In the storm track regions, the differences in LW and SW cloud feedbacks between CAM4 and CAM5 largely cancel. The stratocumulus regions are too small to affect global values. These results are consistent with the changes in cloud forcing in Fig. 4. To understand which parameterization changes to the model are important in these regimes, we next turn to analysis of the modified Cess experiments.

f. Cess experiments

To facilitate comparisons and evaluation of differences between CAM4 and CAM5, we turn to modified Cess experiments with fixed SSTs and specified ΔSST. Modified Cess experiments are run at 2° horizontal resolution and are best compared with the same resolution SOM runs. Table 2 indicates that CAM4-SOM and CAM5-SOM have similar climate sensitivity and global feedbacks for either 1° or 2° resolution. The effective climate sensitivity γ_{eff} in Table 2 differs by 0.2 K between CAM5-SOM2 (2°) and CAM5-Cess (0.3 K for CAM4-SOM2 and CAM4-Cess) but by 0.9 K between CAM4-SOM2 and CAM5-SOM2. Thus, CAM4-Cess and CAM5-Cess have similar feedbacks to their respective SOM runs. Regional patterns of the feedbacks are similar. Ice albedo feedbacks look similar between modified Cess and SOM runs (Fig. 2), even though ice cover change is fixed. Both CAM4 and CAM5 modified Cess experiments position the peak in surface albedo feedback at the latitude of CAM5-SOM since the SST and sea ice perturbations come from this experiment. Water vapor and lapse rate feedbacks are slightly lower in magnitude than SOM experiments in the modified Cess experiments for both CAM4 and CAM5 (Table 2). Differences in cloud feedbacks between CAM4 and CAM5 are nearly the same between the SOM and modified Cess experiments (Fig. 5) at most latitudes in the zonal mean, where shortwave cloud feedbacks are more positive in CAM5 than CAM4 in both SOM and Cess experiments. Note that the modified Cess runs are performed using ΔSST from CAM5 SOM runs.

Maps of adjusted cloud feedbacks (ACF = ALCF + ASCF) for CAM4 and CAM5 from the Cess experiments are shown in Fig. 8. These patterns and their differences are very similar to Figs. 6e and 6f from the SOM runs. Larger positive feedbacks are seen in CAM5-Cess than in CAM4-Cess over the midlatitude ocean storm tracks, and negative feedbacks in the stratocumulus regions in CAM4-Cess have been substantially reduced in CAM5-Cess. Tropical and midlatitude differences stand out. Midlatitude differences are slightly larger in the modified Cess runs (Fig. 8) than in the SOM experiments (Fig. 6). This is also evident in Fig. 5. In summary, the modified

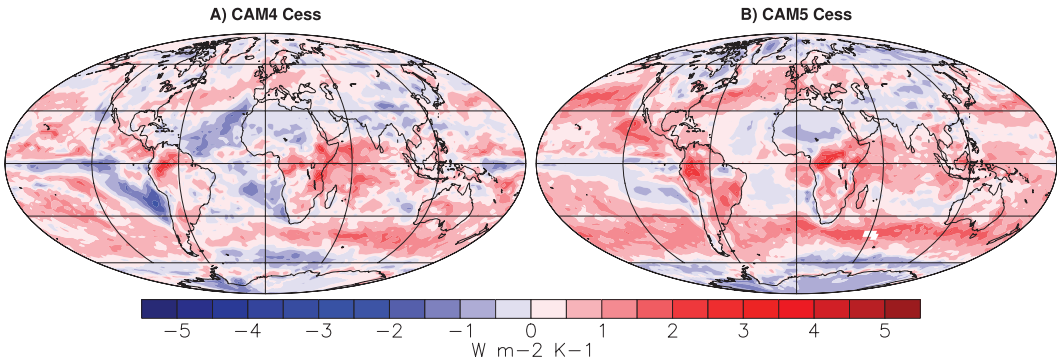

FIG. 8. Adjusted cloud feedback (ACF = ASCF + ALCF) (W m^{-2} K^{-1}) from (a) CAM4-Cess and (b) CAM5-Cess runs.

Cess experiments produce climate feedbacks very similar to comparable SOM runs, and the differences in feedbacks between CAM4 and CAM5 are reproduced in modified Cess runs.

Given the similarities between the modified Cess and SOM runs, we use the modified Cess experiments for diagnosing the parameterizations and regimes responsible for the differences between CAM4 and CAM5. There is a broad progression from more negative to more positive SW cloud feedbacks seen in Table 2, and the total ACF changes from ~0.24 to ~0.41 W m^{-2} K^{-1} in the modified Cess experiments. Higher climate sensitivity γ_{eff} tracks the global averaged ACF. Figure 9 illustrates the zonal mean adjusted cloud feedbacks (ACFs) for the modified Cess cases with different formulations of the atmospheric physics between CAM4 and CAM5 as described in Table 1. The changes in ASCF (Fig. 9a) are dramatic. In the longwave (Fig. 9b) the changes are smaller. There is some compensation between the LW and SW feedbacks (Fig. 9c).

Figure 10 illustrates maps of the progression of ACF from CAM4 (Fig. 10a) through CAM5 (Fig. 10g). Figures 10a and 10g are as in Figs. 8a and 8b. The experiments do not have a linear convergence toward CAM5 because the changes are additive and individual parameterizations have different effects on feedbacks that may be of different sign or interactions that are not additive.

Several features stand out in the cloud feedbacks as the parameterizations change incrementally following Table 1. CAM4 (Fig. 10a) has strong negative feedbacks in the subtropics, including the stratocumulus regions and the flanks of the tropical regions, due to increasing cloud fraction and more negative SW cloud forcing. Stronger positive feedbacks in tropical convective regions are introduced with new microphysics (Fig. 10b), particularly over land—not due to changes in cloud coverage (fraction), but due to a difference in how detrained condensate from convection is partitioned. In the subtropics (particularly the northern subtropics), the cloud

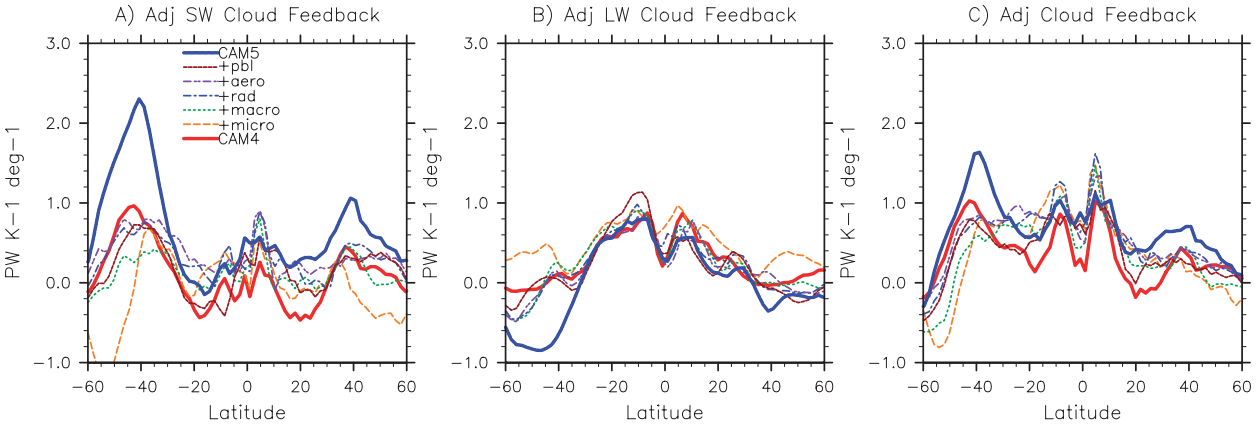

FIG. 9. Zonal-mean ACF (W m^{-2} K^{-1}) for (a) ASCF and (b) ALCF SOM runs corresponding to the CAM4-Cess and CAM5-Cess experiments (thick lines), and intermediate modified Cess experiments (thin lines).

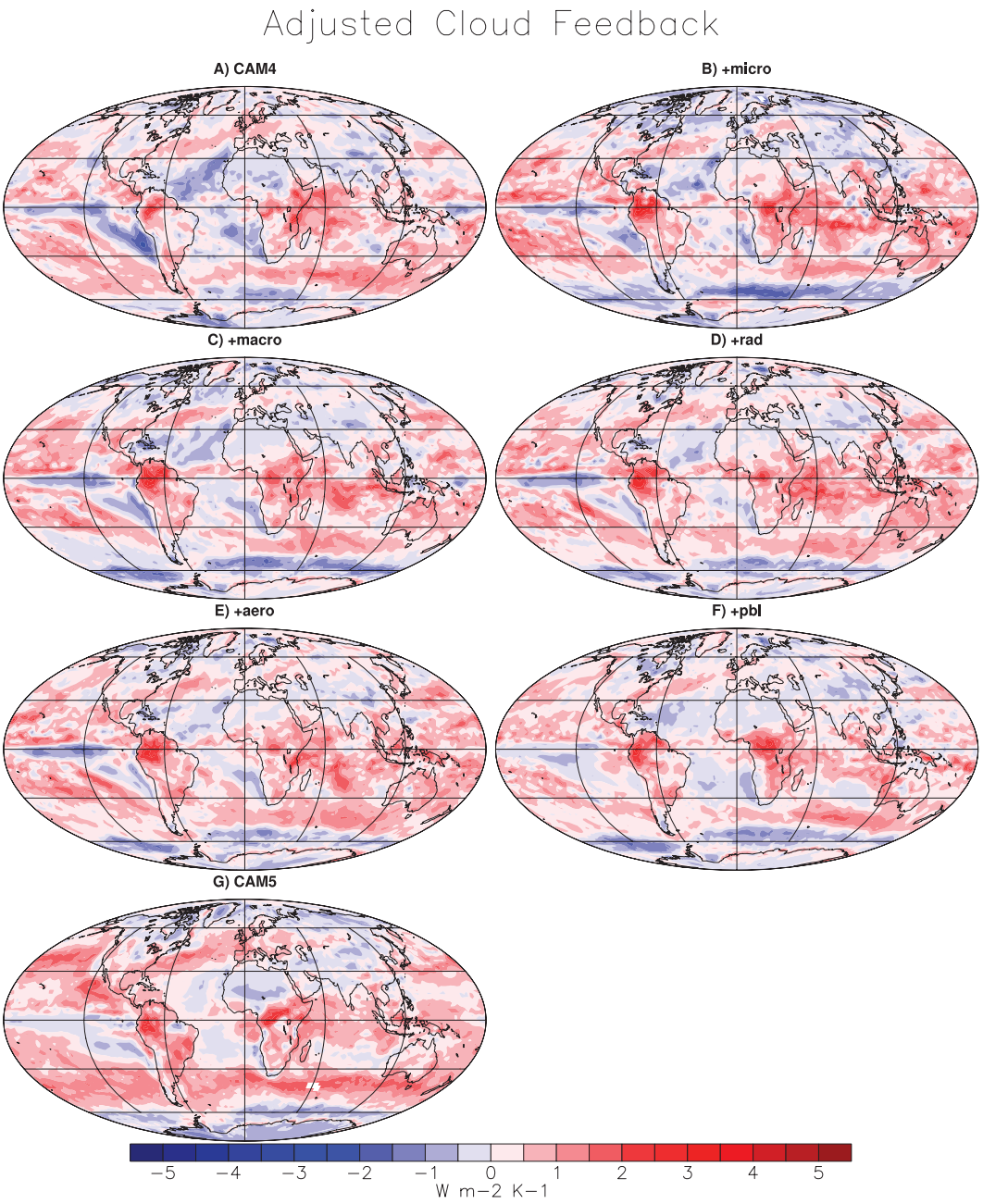

FIG. 10. ACF (W m^{-2} K^{-1}) from modified Cess experiments: (a) CAM4, (b) +micro, (c) +macro, (d) +rad, (e) +aero, (f) +pbl, and (g) +shallow convection (=CAM5).

microphysics change causes the largest increase in ACF (Fig. 9c). This does not show up as a cloud fraction change and is also due to how detrained condensate is treated (increased optical thickness owing to smaller particle sizes). The change in cloud microphysics does not strongly impact the climate sensitivity since midlatitude cloud feedbacks on the polar flanks of the storm tracks get more negative (Fig. 10b). This is probably a result of smaller particle sizes for low and middle level stratiform cloud.

Adding the macrophysics (stratiform cloud fraction scheme) reduces negative feedbacks in the subtropical stratocumulus and at midlatitudes (Fig. 10c). The cloud fraction response is muted (little change in stratus cloud area occurs). A separate climate sensitivity test was performed using CAM4-SOM without the Klein and Hartmann (1993) parameterization for stratocumulus cloud fraction used in the CAM4 macrophysics. Cloud feedbacks do not show any difference from standard

TABLE 3. Feedbacks (λ_X; W m^{-2} K^{-1}), ALCF and ASCF and climate sensitivity (γ_{eff}; K) from sensitivity runs as described in the text.

Simulation	λ_α	λ_{Ts}	λ_{Tp}	λ_{LR}	λ_Q	ALCF	ASCF	γ_{eff}
CAM5-Cess 10 yr	0.29	−0.64	−2.21	−0.15	1.32	−0.05	0.46	4.4
CAM5-Cess 5 yr	0.28	−0.64	−2.22	−0.16	1.33	−0.03	0.42	4.4
CAM5-Cess ΔSST4	0.23	−0.65	−2.21	−0.15	1.33	−0.01	0.55	4.8
CAM5-Cess fixed aero	0.29	−0.64	−2.21	−0.14	1.33	−0.01	0.34	4.5
+pbl $RH_c = 0.95$	0.31	−0.64	−2.21	−0.15	1.31	0.15	0.10	2.9
+pbl $RH_c = 0.91$	0.31	−0.64	−2.22	−0.16	1.32	0.15	0.02	2.7
+micro $RH_c = 0.92$	0.31	−0.64	−2.21	−0.16	1.34	0.32	0.08	2.7
+micro $RH_c = 0.88$	0.31	−0.64	−2.21	−0.15	1.35	0.34	−0.14	2.4

CAM4-SOM, consistent with the small stratocumulus area (Fig. 7).

Introducing the radiation code and cloud optics makes tropical cloud feedbacks (Fig. 10d) more positive in the Indian Ocean. This appears to be due to a LW cloud forcing change resulting from changes in the ice cloud optics. The global climate sensitivity increases substantially (Table 2) because of a jump in the shortwave (and total) cloud feedbacks (Table 2). The sensitivity also increases because offline calculations (Kay et al. 2011, manuscript submitted to *J. Climate*) show an increase in the CO_2 radiative forcing G_{CO_2} of about 10% (from 3.5 to 3.8 W m^{-2} for doubling CO_2 from 280 to 560 ppmv) with the Rapid Radiative Transfer Model for GCMs radiation code.

The introduction of the aerosol scheme and new aerosol optics (that alter the direct radiative effect of aerosols) does not have a strong impact on cloud feedback (Figs. 10e) or overall climate sensitivity (Table 2). This assumes constant aerosol emissions for present-day conditions.

The new boundary layer scheme increases negative feedbacks in the subtropics and tropics (Figs. 10f and 9c). This occurs in the subtropics, mostly in the SW (Fig. 9a), because of larger increases in low-cloud fraction in the subtropics with the addition of the new PBL scheme. This increase enhances negative SW cloud feedbacks and corresponds to the only large decrease in the climate sensitivity in the progression between CAM4 and CAM5 (Table 2).

The introduction of the shallow cumulus scheme is the last piece that makes up CAM5, and its introduction has the largest impact on ACF (difference between Figs. 10f and 10g). The effects are largest in the oceanic midlatitude storm tracks and extend to the edge of the subtropics. Effects are due to cloud fraction changes (reductions) extending farther equatorward in these simulations. Differences are also clear in the zonal mean (Fig. 9). The reductions in cloud cause increases in ASCF in the storm tracks (Fig. 9a) and are consistent with a larger reduction in the shallow convection mass flux for the $2 \times CO_2$ case in CAM5 over CAM4.

5. Sensitivity tests

We perform several experiments, documented in Table 3, to further clarify the aforementioned results. First, we recalculate feedbacks from the CAM5 modified Cess experiment using only 5 years of data. The feedbacks are essentially the same (Table 3) as when calculated with 10 years of output, indicating that statistically 5 years is sufficient to eliminate the effects of interannual variability. For the SOM experiments, we have analyzed both 10 and 20 years of output and also found similar agreement. We also evaluated feedbacks if we use the ΔSST from the CAM4 SOM run (ΔSST in Table 3). The feedbacks (Table 3) are very similar but with slightly higher climate sensitivity (γ) due to more positive ASCF: the patterns are similar (not shown).

An experiment was performed using CAM5-Cess with fixed aerosol concentrations (fixed aero in Table 3). This eliminates any potential feedback between aerosol concentrations and climate. The results of a feedback analysis in Table 3 are nearly identical to the base case CAM5 experiment with similar climate sensitivity. However, there is a decrease in ACF (ASCF + ALCF). The decrease in ACF is mostly due to ASCF in Northern Hemisphere midlatitudes, indicating that, when aerosol concentrations are allowed to interact with the clouds, such as through changes to aerosol scavenging (lifetime), it can affect SW cloud feedbacks. However, the interaction does not seem to alter global climate sensitivity.

We also use two interim adjustment experiments to evaluate the effect of single parameter changes on the simulations. Here we modify the critical relative humidity for the formation of low clouds in CAM5 (RH_c). In the CAM code, this is the variable ''rhminl'' in the parameterization of Slingo (1989). This is done in two simulations, when the microphysics is altered (+micro) and when the new boundary layer scheme is introduced (+pbl). The lower ''RH_c'' runs in Table 3 are significantly out of TOA radiative balance, with much larger cloud fractions and cloud forcing than observed. Lowering RH_c generally increases cloud fraction and cloud

forcing. The runs with larger cloud fraction (lower RH_c) and larger cloud forcing have reduced ASCF and reduced climate sensitivity. In both of these cases, thicker low clouds (higher gross SW cloud forcing) tend to lower climate sensitivity (γ_{eff}) in these CAM5-Cess simulations.

In summary, the feedback calculations are robust with respect to the time period and input SST used. We also note from Table 2 that feedbacks are not affected by horizontal resolution in the CAM4 and CAM5 SOM runs. Aerosols appear to have a small impact on SW cloud feedbacks, but not climate sensitivity. The diagnosis of feedbacks also appears fairly stable to some of the more commonly used gross cloud adjustment parameters in climate models, with the caveat that the changes to clouds may matter for climate sensitivity, and higher mean cloud forcing results in decreased ASCF and lower climate sensitivity.

6. Discussion

A series of experiments has been conducted to try to understand what processes and regions are responsible for the change in cloud feedbacks between two versions of CAM. Model configurations with fixed ocean temperature perturbations derived from coupled slab ocean model runs are able to reproduce feedbacks in the SOM experiments, allowing us to use the less computationally intensive modified Cess experiments (following Cess et al. 1990). Modified Cess experiments can reproduce key climate feedbacks seen in SOM runs, in contrast to traditional Cess experiments (Senior and Mitchell 1993; Ringer et al. 2006). Furthermore, global climate sensitivity and climate feedbacks do not appear sensitive to model horizontal resolution (1° or 2°) in either CAM4 or CAM5.

CAM5 has a higher climate sensitivity than CAM4. Water vapor, temperature, and lapse rate feedbacks as well as surface albedo feedbacks are basically the same between the two models. The difference in sensitivity is mostly due to (i) changes in cloud feedbacks and (ii) a difference in G_{CO_2} between CAM4 and CAM5. The G_{CO_2} is a function of the model state (e.g., the temperature, cloud, and water vapor distribution) and the radiative transfer code. Calculations (see Kay et al. 2011, manuscript submitted to *J. Climate*) indicate $G_{\text{CO}_2} = 3.5\ \text{W m}^{-2}$ for CAM4 and $3.8\ \text{W m}^{-2}$ for CAM5. The result is consistent with calculations by Iacono et al. (2008), who indicate that the difference is due to the radiative transfer code itself (not model state). Assuming a constant total feedback strength (λ) of $-1\ \text{W m}^{-2}\ \text{K}^{-1}$ in Eq. (2), this yields a difference in climate sensitivity (ΔT_{as}) of 0.3 K, or about 40% of the 0.8-K difference in sensitivity between CAM4-SOM and CAM5-SOM (Table 2).

There is uncertainty that comes into the nonlinear term (NT) in Eq. (3): NT can be calculated by estimating the total feedback (λ) for CAM4 and CAM5 as λ_{eff} [Eq. (5)] with G_{CO_2} differing for CAM4 and CAM5, and ΔT_{as} and H as the difference in temperature and TOA balance, respectively, between the 2 × CO2 and 1 × CO2 SOM runs. This allows a closed sum of feedbacks. For CAM5-SOM $H = -0.005\ \text{W m}^{-2}$, so $\lambda_{\text{eff}} = (3.8 - 0.005)/4.0 = -0.95\ \text{W m}^{-2}\ \text{K}^{-1}$. For CAM4-SOM $H = -0.075$, so $\lambda_{\text{eff}} = (3.5 - 0.075)/3.2 = -1.07\ \text{W m}^{-2}\ \text{K}^{-1}$.

The sum of the feedbacks from Table 2 does not equal this (−0.92 for CAM4-SOM, −0.91 for CAM5-SOM) This means that the nonlinear term NT = +0.04 for CAM5-SOM and +0.15 for CAM4-SOM. This is a measure of the uncertainty and, for CAM4, is larger than the 10% estimate of Shell et al. (2008). The clouds differ by $0.08\ \text{W m}^{-2}\ \text{K}^{-1}$ (with CAM5 higher). This is offset by differences of −0.03 and −0.06 in albedo and Planck feedbacks, representing small fractional changes in these feedbacks (9% and 3%, respectively). There is 10%–20% uncertainty in the feedbacks due to NT.

After factoring in the change in radiative forcing, cloud feedbacks account for much of the remaining difference between the climate sensitivity in CAM4 and CAM5 and the largest percent difference in feedbacks (25%). The $0.08\ \text{W m}^{-2}\ \text{K}^{-1}$ difference in net cloud feedback between CAM4-SOM and CAM5-SOM masks larger changes in SW (+0.29) and LW (−0.21) components, indicating a very different cloud response in CAM5 from CAM4. Using perturbations to Eq. (3), the net cloud feedback difference of $0.08\ \text{W m}^{-2}\ \text{K}^{-1}$ between CAM5-SOM and CAM4-SOM accounts for another ~0.26–0.37 K (30%–50%) of the difference in climate sensitivity, depending on whether CAM4 or CAM5 values of G_{CO_2} and λ_{eff} are used in Eq. (3).

The changes in cloud feedbacks are spatially coherent. Negative cloud feedbacks in the tropics decrease in the CAM5 experiments, while positive cloud feedbacks increase over the subtropics and in the storm track regions. Tropical changes are due to reductions in negative feedbacks with a new cloud microphysics and macrophysics scheme. The microphysics affects convective detrainment, and the macrophysics mutes cloud fraction changes in trade cumulus regimes in the subtropics. The new PBL scheme tends to increase negative cloud feedbacks through increased subtropical cloud fraction and reduce climate sensitivity, counteracting the changes from the microphysics. In the subtropics and midlatitudes, positive increases of cloud forcing in the equatorward portion of the stormtrack regions (due to larger decreases in cloud fraction) occur with the

introduction of the new shallow convection (cumulus) scheme, enhancing climate sensitivity. The new shallow cumulus scheme alters the interaction between stratus and shallow cumulus clouds and has a major effect on the flanks of the storm tracks. Larger decreases in shallow convective mass flux are occurring in CAM5 for $2 \times CO2$ conditions, decreasing cloud in broad regions as the storm tracks shift poleward. The poleward shift in the $2 \times CO_2$ simulations is consistent with observations (Seidel et al. 2008) and other model simulations (Son et al. 2009) and is about the same in both CAM4 and CAM5, but the effect on clouds is larger in CAM5.

Notably, these changes are not strongly due to the subtropical marine stratocumulus regions. When cloud feedbacks are weighted by area, these regions are less important as they represent only 2%–6% of the area of the planet. These small regions may be more important in a fully coupled system with ocean dynamics, yet given their limited area the stratocumulus region impact on global feedback strength is inherently limited. From these experiments it appears that cumulus clouds in the subtropics and storm track regions exert the strongest lever on global climate sensitivity. This conclusion is supported by previous work. Bony et al. (2004) noted that it was regions of moderate subsidence (trade cumulus) that have the highest frequency and largest effect on tropical averaged cloud forcing, and Medeiros et al. (2008) found that the shallow cumulus regime was most important for cloud forcing and feedback. While Williams and Webb (2009) stress the importance of low clouds for cloud feedback, half of their global signal is from outside of the tropical regions. The results are consistent with recent work by Trenberth and Fasullo (2010), who found a relationship between cloudiness in the SH storm track (a canonical bias in models) and model climate sensitivity.

In the CAM5 simulations, as the planet warms, low clouds become less extensive and the storm tracks move poleward. The change in cloudiness and cloud forcing is most strongly impacted by shallow convective clouds and is strongly correlated with decreases in shallow convective mass flux. One likely mechanism is that the reduced mass flux alters detrainment into stratiform clouds, reducing the liquid water path and allowing for a larger change (reduction) in the (negative) cloud forcing.

Perturbation tests reveal two additional important features of the simulations. First, tests at two different points in the model development process indicated that climate sensitivity does appear to be coherently decreased by ~10% as cloud forcing increases. In these experiments, a climate state with more cloud radiative forcing (thicker clouds with more water substance and/or larger horizontal extent) implies a smaller percentage change in cloud forcing response and lower climate sensitivity. This is likely due to the nonlinear effects of radiative transfer: bands where cloud is important in the LW and SW saturate, and further changes to cloud forcing are reduced with increased cloudiness. Expanding on this hypothesis, high water content clouds can especially dampen warming over an ice-covered ocean. Kay et al. (2011, manuscript submitted to *J. Climate*) find that the high water content Arctic clouds in CAM4 dampen greenhouse warming both with negative Arctic shortwave cloud feedbacks and by masking the surface, reducing positive surface albedo feedbacks.

Second, fixing aerosol concentrations in CAM5-Cess decreased SW cloud feedbacks. The decreased feedback implies that interactive prognostic aerosols play a role in understanding cloud feedback responses; however, the effects on climate sensitivity are not conclusive, and the results are not seen with the introduction of the new aerosol scheme (Table 2). This may indicate a complex interaction of several different parameterizations between clouds and aerosols.

7. Conclusions

This work highlights the evolution of climate sensitivity in CAM from version 4 (3.2 K) to version 5 (4.0 K). It also highlights the utility of modified ''Cess'' experiments to diagnose feedbacks. The increase in sensitivity is due to changes in CO_2 radiative forcing (40%) and most of the remainder is due to changes in cloud feedbacks. Changes in cloud feedbacks primarily occur in the tropics and midlatitudes. Changes to water vapor, lapse rate, and albedo feedbacks are not strong contributors to changes in global climate sensitivity between CAM4 and CAM5.

Several parameterizations contribute to cloud changes in the tropics and a reduction of negative feedbacks in the subtropics. The shallow cumulus scheme is important for enhancing positive cloud feedbacks in the subtropics and midlatitudes. The equatorward branches of the storm tracks and deep convective regions contribute most to the global change in cloud feedbacks. Stratocumulus regions in the tropics and subtropics do not strongly contribute to the change in cloud feedbacks or climate sensitivity. Further work will be necessary to understand the exact mechanisms that alter the climate sensitivity.

These results hint at relationships between clouds and climate sensitivity. CAM4 and CAM5 span a wide range of structural parameterization differences. In perturbation experiments, climate states with higher cloud forcing are less sensitive than those with thinner clouds. This

may be location and regime specific. Further work is necessary to (i) test these conclusions across a broader spectrum of models and (ii) compare model states with observations of key cloud parameters to attempt to better constrain climate sensitivity. Current observational constraints imply cloud feedbacks similar to what is described here (Dessler 2010), but do not have sufficient precision to constrain climate sensitivity. Given the current uncertainty in global estimates of important cloud properties, it is critical to get better observations (both mean state and variability) in different regions (such as the subtropics and the Southern Ocean).

Acknowledgments. KMS was supported by the National Science Foundation Grant ATM-0904092. Thanks are given to C. Hannay for assistance with runs and J. T. Kiehl for key insights. We also thank B. Medieros, K. E. Trenberth, and J. T. Fasullo for discussions.

REFERENCES

Bitz, C., K. Shell, P. Gent, D. Bailey, G. Danabasoglu, K. Armour, M. Holland, and J. Kiehl, 2012: Climate sensitivity of the Community Climate System Model version 4. *J. Climate,* in press.

Bony, S., and J.-L. Dufresne, 2005: Marine boundary layer clouds at the heart of tropical cloud feedback uncertainties in climate models. *Geophys. Res. Lett.,* **32,** L20806, doi:10.1029/2005GL023851.

——, ——, H. Le Treut, J.-J. Morcrette, and C. Senior, 2004: On dynamic and thermodynamic components of cloud changes. *Climate Dyn.,* **22,** 71–86, doi:10.1007/s00382-003-0369-6.

——, and Coauthors, 2006: How well do we understand and evaluate climate change feedback processes? *J. Climate,* **19,** 3445–3482.

Bretherton, C. S., and S. Park, 2009: A new moist turbulence parameterization in the Community Atmosphere Model. *J. Climate,* **22,** 3422–3448.

Cess, R. D., and Coauthors, 1990: Intercomparison and interpretation of climate feedback processes in 19 atmospheric general circulation models. *J. Geophys. Res.,* **95,** 16 601–16 615.

——, and Coauthors, 1996: Cloud feedback in atmospheric general circulation models: An update. *J. Geophys. Res.,* **101** (D8), 12 791–12 794.

Collins, W. D., and Coauthors, 2004: Description of the NCAR Community Atmosphere Model (CAM 3.0). NCAR Tech. Note NCAR/TN-464+STR, 226 pp.

——, and Coauthors, 2006: The formulation and atmospheric simulation of the Community Atmosphere Model Version 3 (CAM3). *J. Climate,* **19,** 2122–2161.

Colman, R., 2003: A comparison of climate feedbacks in general circulation models. *Climate Dyn.,* **20,** 865–873.

Dessler, A. E., 2010: A determination of the cloud feedback from climate variations over the past decade. *Science,* **330,** 1523–1527, doi:10.1126/science.1192546.

Easter, R. C., and Coauthors, 2004: MIRAGE: Model description and evaluation of aerosols and trace gases. *J. Geophys. Res.,* **109,** D20210, doi:10.1029/2004JD004571.

Gettelman, A., and Coauthors, 2010: Global simulations of ice nucleation and ice supersaturation with an improved cloud scheme in the Community Atmosphere Model. *J. Geophys. Res.,* **115,** D18216, doi:10.1029/2009JD013797.

Gregory, J. M., and Coauthors, 2004: A new method for diagnosing radiative forcing and climate sensitivity. *Geophys. Res. Lett.,* **31,** L03205, doi:10.1029/2003GL018747.

Held, I. M., and B. J. Soden, 2000: Water vapor feedback and global warming. *Annu. Rev. Energy Environ.,* **25,** 441–475.

Hurrell, J. W., J. J. Hack, D. Shea, J. M. Caron, and J. Rosinski, 2008: A new sea surface temperature and sea ice boundary dataset for the Community Atmosphere Model. *J. Climate,* **21,** 5145–5153.

Iacono, M. J., J. S. Delamere, E. J. Mlawer, M. W. Shephard, S. A. Clough, and W. D. Collins, 2008: Radiative forcing by long-lived greenhouse gases: Calculations with the AER radiative transfer models. *J. Geophys. Res.,* **113,** D13103, doi:10.1029/2008JD009944.

Kiehl, K. T., C. A. Shields, J. J. Hack, and W. D. Collins, 2006: The climate sensitivity of the Community Climate System Model version 3 (CCSM3). *J. Climate,* **19,** 2584–2596.

Klein, S. A., and D. L. Hartmann, 1993: The seasonal cycle of low stratiform clouds. *J. Climate,* **6,** 1587–1606.

Liu, X., and Coauthors, 2011: Toward a minimal representation of aerosol direct and indirect effects: Model description and evaluation. *Geosci. Model Dev. Discuss.,* **4,** 3485–3598.

Medeiros, B., and B. Stevens, 2011: Revealing differences in GCM representations of low clouds. *Climate Dyn.,* **36,** 385–399, doi:10.1007/s00382-009-0694-5.

——, ——, I. M. Held, M. Zhao, D. L. Williamson, J. G. Olson, and C. S. Bretherton, 2008: Aquaplanets, climate sensitivity, and low clouds. *J. Climate,* **21,** 4974–4991.

Morrison, H., and A. Gettelman, 2008: A new two-moment bulk stratiform cloud microphysics scheme in the Community Atmosphere Model, version 3 (CAM3). Part I: Description and numerical tests. *J. Climate,* **21,** 3642–3659.

Neale, R. B., J. H. Richter, and M. Jochum, 2008: The impact of convection on ENSO: From a delayed oscillator to a series of events. *J. Climate,* **21,** 5904–5924.

——, and Coauthors, 2010: Description of the NCAR Community Atmosphere Model (CAM5.0). NCAR Tech. Note NCAR/TN-486-STR, 268 pp.

Park, S., and C. S. Bretherton, 2009: The University of Washington shallow convection and moist turbulence schemes and their impact on climate simulations with the Community Atmosphere Model. *J. Climate,* **22,** 3449–3469.

Ramanathan, V., R. D. Cess, E. F. Harrison, P. Minnis, B. R. Barkstrom, E. Ahmad, and D. Hartmann, 1989: Cloud-radiative forcing and climate: Results from the Earth Radiation Budget Experiment. *Science,* **243,** 57–63.

Ringer, M. A., and Coauthors, 2006: Global mean cloud feedbacks in idealized climate change experiments. *Geophys. Res. Lett.,* **33,** L07718, doi:10.1029/2005GL025370.

Santer, B. D., and Coauthors, 2005: Amplification of surface temperature trends and variability in the tropical atmosphere. *Science,* **309,** 1551–1556, doi:10.1126/science.1114867.

Schneider, S., 1972: Cloudiness as a global climatic feedback mechanism: The effects on radiation balance and surface temperatures of variations in cloudiness. *J. Atmos. Sci.,* **29,** 1413–1422.

Seidel, D. J., Q. Fu, W. J. Randel, and T. Reichler, 2008: Widening of the tropical belt in a changing climate. *Nat. Geosci.,* **1,** 21–24, doi:10.1038/ngeo.2007.38.

Senior, C. A., and J. F. B. Mitchell, 1993: Carbon dioxide and climate: The impact of cloud parameterization. *J. Climate,* **6,** 393–418.

Shell, K. M., J. T. Kiehl, and C. A. Shields, 2008: Using the radiative kernel technique to calculate climate feedbacks in NCAR's Community Atmosphere Model. *J. Climate,* **21,** 2269–2282.

Slingo, A. A., 1989: A GCM parameterization for the shortwave radiative properties of clouds. *J. Atmos. Sci.,* **46,** 1419–1427.

Soden, B. J., and I. M. Held, 2006: An assessment of climate feedbacks in coupled ocean–atmosphere models. *J. Climate,* **19,** 3354–3360.

——, D. D. Turner, B. M. Lesht, and L. M. Miloshevich, 2004: An analysis of satellite, radiosonde, and lidar observations of upper tropospheric water vapor from the Atmospheric Radiation Measurement Program. *J. Geophys. Res.,* **109,** D04105, doi:10.1029/2003JD003828.

——, I. M. Held, R. Colman, K. M. Shell, J. T. Kiehl, and C. A. Shields, 2008: Quantifying climate feedbacks using radiative kernels. *J. Climate,* **21,** 3504–3520.

Solomon, S., D. Qin, M. Manning, M. Marquis, K. Averyt, M. M. B. Tignor, H. L. Miller Jr., and Z. Chen, Eds., 2007: *Climate Change 2007: The Physical Science Basis*. Cambridge University Press, 996 pp.

Son, S.-W., and Coauthors, 2009: The impact of stratospheric ozone recovery on tropopause height trends. *J. Climate,* **22,** 429–445.

Stephens, G. L., 2005: Cloud feedbacks in the climate system: A critical review. *J. Climate,* **18,** 237–273.

Trenberth, K. E., and J. T. Fasullo, 2010: Simulation of present-day and twenty-first-century energy budgets of the southern oceans. *J. Climate,* **23,** 440–454.

Webb, M. J., and Coauthors, 2006: On the contribution of local feedback mechanism to the range of climate sensitivity in two GCM ensembles. *Climate Dyn.,* **27,** 17–38, doi:10.1007/s00382-006-0111-2.

Wetherald, R. T., and S. Manabe, 1988: Cloud feedback processes in a general circulation model. *J. Atmos. Sci.,* **45,** 1397–1415.

Williams, K. D., and M. J. Webb, 2009: A quantitative performance assessment of cloud regimes in climate models. *Climate Dyn.,* **33,** 141–157, doi:10.1007/s00382-008-0443-1.

Zhang, M. H., J. J. Hack, and J. T. Kiehl, 1994: Diagnostic study of climate feedback processes in atmospheric general circulation models. *J. Geophys. Res.,* **99** (D3), 5525–5537.